Published in final edited form as:
AIMS Biophys. 2020 ; 7(3): 144–166. doi:10.3934/biophy.2020012.

Imaging flow cytometry methods for quantitative analysis of label-free crystalline silica particle interactions with immune cells

Bradley Vis, **Jonathan J. Powell**, **Rachel E. Hewitt***
Biomineral Research Group, Department of Veterinary Medicine, University of Cambridge, Madingley Rd, Cambridge CB3 0ES, UK

Abstract

Exposure to respirable fractions of crystalline silica quartz dust particles is associated with silicosis, cancer and the development of autoimmune conditions. Early cellular interactions are not well understood, partly due to a lack of suitable technological methods. Improved techniques are needed to better quantify and study high-level respirable crystalline silica exposure in human populations. Techniques that can be applied to complex biological matrices are pivotal to understanding particle-cell interactions and the impact of particles within real, biologically complex environments. In this study, we investigated whether imaging flow cytometry could be used to assess the interactions between cells and crystalline silica when present within complex biological matrices. Using the respirable-size fine quartz crystalline silica dust Min-u-sil® 5, we first validated previous reports that, whilst associating with cells, crystalline silica particles can be detected solely through their differential light scattering profile using conventional flow cytometry. This same property reliably identified crystalline silica in association with primary monocytic cells *in vitro* using an imaging flow cytometry assay, where darkfield intensity measurements were able to detect crystalline silica concentrations as low as 2.5 μg/mL. Finally, we ultilised fresh whole blood as an exemplary complex biological matrix to test the technique. Even after the increased sample processing required to analyse cells within whole blood, imaging flow cytometry was capable of detecting and assessing silica-association to cells. As expected, in fresh whole blood exposed to crystalline silica, neutrophils and cells of the monocyte/macrophage lineage phagocytosed the particles. In addition to the use of this technique in *in vitro* exposure models, this method has the potential to be applied directly to *ex vivo* diagnostic studies and research models, where the identification of crystalline silica association with cells in complex biological matrices such as bronchial lavage fluids, alongside additional functional and phenotypic cellular readouts, is required.

Keywords

crystalline silica particles; quartz dust; imaging flow cytometry; macrophages; neutrophils; phagocytes; label-free

***Correspondence**: reh63@cam.ac.uk; Tel: +441223426356; Fax: +01223437515.

Conflict of interest
The authors declare no conflicts of interest.

Europe PMC Funders Author Manuscripts

Europe PMC Funders Author Manuscripts

1 Introduction

Quartz is a common form of crystalline silica and is a major component of rocks, sands, and soils [1]. Exposure to quartz most commonly occurs during occupational activities involving the movement of earth, disturbance of silica-containing products, or during use or manufacturing of silica-containing products. Respirable size crystalline silica dust particles are defined as particles around 10 μm in diameter and under, but are primarily considered to be outside of the nanoparticulate size range [2]. Respirable silica particles generated during occupational activities are inhaled and deposited in the lung. Epidemiological studies have shown that inhalation of quartz dust is associated with silicosis, lung cancer, and pulmonary tuberculosis [3]. After inhalation and deposition in lung alveoli, macrophages phagocytose the crystalline silica particles and an inflammatory response is induced which, in turn, stimulates a process termed silicosis [4]. In addition to the development of silicosis, chronic exposure to crystalline silica increases the prevalence of several autoimmune states, including systemic sclerosis, rheumatoid arthritis and anti-neutrophil cytoplasmic antibody-related vasculitis [5]. Despite substantial links between the autoimmune states and crystalline silica dust exposure, the role of the particles in the initiation and development of autoimmunity is not well understood [4,6–9]. The lack of understanding is due, in part, to a lack of animal models that precisely mimic human autoimmune disease development [10], and the considerable extent of time between particle exposure and the diagnosis of autoimmune disease. The multiple complexities and challenges in investigating exposures involving small particulates [11–13], and the limitations of using cell lines for *in vitro* studies [14], remain as considerable experimental obstacles for particulate studies. Investigations into initial interactions of primary innate human cells with crystalline silica particles within realistic biological matrices or directly *ex vivo* are desirable but limited in number [15]. Methodology for characterising particle-cell interactions is often in the form of qualitative imaging (*i.e.,* observational microscopy), while robustly quantitative techniques, such as conventional flow cytometry, lack detailed information regarding the nature of interactions. However, advances in the fields of microscopy and imaging flow cytometry have now made it possible to generate fully quantitative imaging analyses that can detail the interactions and effects of micron and nano-sized particles *in vitro* and *ex-vivo* on primary cell populations [16–21]. Such techniques may assist in understanding the immunologic events which ultimately lead to autoimmune states initiated by exposure to respiratory fractions of crystalline silica.

Imaging flow cytometry combines high definition microscopy with high throughput flow cytometry, making it a useful tool for detailed examination of particle-cell events [17–21]. The interactions of crystalline silica with cells have been identified using microscopy [22–23] and silica's general association to cells has been characterized by light scattering intensity using conventional flow cytometry [24–25]. These studies would suggest that the light scattering properties of crystalline silica particles can also be visualized, label-free, using imaging flow cytometry. Using this technique, the visualization of crystalline silica association with cells obtained from bronchial washings, blood or other tissue digests might be possible, if the material is present in sufficient quantities. Additionally, this technique could also be applied to *in vitro* studies using primary cells in physiologically relevant

matrices or cell lines. In this current study, we aimed to establish whether imaging flow cytometry could be used to detect label-free crystalline silica particles in association with resident blood immune cells and to examine the relationship of crystalline silica with cells in the complex environment of whole blood as an exemplar protein and cell-rich biological matrix. We first utilised peripheral blood mononuclear cells (PBMC) and conventional flow cytometry to examine the ability of crystalline particles to scatter light whilst associating with cells, validating previous observations of differing side scatter (SSC) profiles [24–26]. We then tested the capacity of imaging flow cytometry for label-free identification of crystalline silica particles at decreasing doses in association with phagocytes within PBMC, before moving to the examination of monocyte and neutrophil cell populations present in whole blood, in a fully quantitative fashion.

2 Materials and methods

2.1 Ethical approval and consent to participate

The study was approved by the UK NHS Health Research Authority, West Midlands – Edgbaston Research Ethics Committee, REC reference 18/WM/0221 and the University of Cambridge, human biology research ethics committee, application HBREC.2015.10. For the investigation of crystalline silica particles association with cells present in whole blood, fresh peripheral blood was obtained from healthy donors following informed written consent.

2.2 Conduct of the study

To enable the investigation of label-free identification of crystalline silica in resident blood cells, PBMC were isolated from fresh, surplus-to-requirement leukocyte cones (National Blood Service, Cambridge, UK) using Lymphoprep (Axis Shield Diagnostics Ltd, Scotland) and density gradient centrifugation. For the investigation of crystalline silica particle-association with cells present in whole blood, fresh peripheral blood was obtained from healthy donors following informed consent. Incubations with crystalline silica and analyses of the cellular interactions were then carried out as described in the following sections.

2.3 Preparation and size characterisation of crystalline silica

Min-u-sil® 5, previously identified as quartz silica [1], was acquired from US Silica Company. The crystalline powder was baked at 200 °C (to break down any endotoxins) prior to suspending in sterile H_2O (Sigma-Aldrich, W3500), as conducted previously [27]. Under sterile, controlled conditions, the powder was suspended in tissue culture grade water and the suspension completely dispersed prior to sizing and addition to cell culture media. Particle size of the suspension was assessed with a Malvern Mastersizer 2000 (Malvern Instruments), using parameters for silicon oxide (refractive index = 1.45, absorption = 0.01). Supplementary Figure 1 shows the particle size distribution of the crystalline silica. The particles are not nanoparticulate but ranged from 0.25 to 12 μm in size, with a mean diameter of 2.6 μm, covering the range of particle sizes to which humans are exposed [28].

2.4 PBMC isolation, culture and fluorescent antibody staining

Human PBMC isolates from fresh leukocyte cones were washed in RPMI media, counted and re-suspended in freezing medium for cryogenic storage until use. Prior to experimentation, PBMC were thawed, washed and rested in tissue culture medium (TCM, RPMI supplemented with 10% foetal bovine serum, 2 mM L-glutamine, 100 U/ml penicillin and 100 μg/ml streptomycin (Sigma-Aldrich, UK)) containing DNase (10 ng/mL) for 2 h. PBMC were then counted, re-suspended in TCM, and incubated with 0–100 μg/mL (parts per million, ppm) crystalline silica for 24 h, at 37 °C, with 5% CO_2. Subsequent to incubation with crystalline silica, PBMC were washed and re-suspended in ~200 μL ice-cold phosphate-buffered saline (PBS) containing 1% bovine serum albumin (BSA) wash buffer ("wash buffer"). Cells were then stained for 20 min on ice in the dark with APC-conjugated anti-CD11c and FITC-conjugated anti-CD3 (BD Biosciences, UK), or Alexa 488 conjugated anti-CD14 (BD Biosciences, UK). To distinguish viability, the dead/dying cell stain 7-AAD (Life technologies, UK), was added to the cells after surface antibody staining and cells were incubated at room temperature for 10 min. After staining, PBMC were washed again with wash buffer and re-suspended in a small volume of PBS containing 2% paraformaldehyde (PFA) and placed on ice in the dark until acquisition. Single stain compensation tubes and unstained PBMC tubes, with and without crystalline silica were also prepared at this time from PBMC samples to compensate for spectral overlap.

2.5 Whole blood culture, red blood cell lysis, fluorescent antibody staining

Fresh whole blood (WB) was collected into tubes containing lithium-heparin and briefly mixed within the tubes. WB was then promptly transferred to Falcon tubes and heparin (tissue culture grade heparin sodium salt dissolved in tissue culture grade H_2O, both from Sigma, UK) was added to a final concentration of 0.5 mg/mL. WB (up to 200 μL) was transferred to sterile FACS tubes, treated with 0–250 μg/mL crystalline silica, and incubated for 24 h at 37 °C, with 5% CO_2. Cultures were placed on a gentle shaker to prevent settling and blood separation. Unchallenged cells were set up alongside the negative control for each subject. Following incubation, the red blood cells were lysed with BD Pharm Lyse (BD Biosciences, UK) according to manufacturers' instructions. After lysing, the supernatants were carefully aspirated, taking care not to disrupt white blood cell pellets, and the pellets were washed twice in cold tissue culture grade dPBS and once with cold wash buffer, centrifuging down the cell pellet between washes. Cells were then stained for 20 min on ice in the dark with the cell surface antibodies (FITC or Alexa 488 conjugated anti CD14, and PE-conjugated anti CD16b, (BD Biosciences, UK)) at manufactures' recommended volumes added to the residual wash buffer (around 200 μL). After staining, the cells were washed again with cold wash buffer and were re-suspended in a small volume of PBS containing 2% PFA. Cultures were stored on ice in the dark until acquisition.

2.6 Conventional flow cytometry

Flow cytometry was performed using a CyAn ADP 9 colour analyser (Beckman Coulter, UK) equipped with 405 nm, 488 nm and 642 nm solid-state lasers and 11 detectors in standard configuration. Summit software was used for both acquisition and analysis (Beckman Coulter, UK). Prior to acquisition, the machine was calibrated with single peak

alignment beads (Spherotech, USA), checking that coefficients of variation resided within the target ranges. Samples were filtered through 35 μm nylon cell strainer mesh tubes (BD Biosciences, UK) immediately prior to acquisition and a minimum of 250,000 events were acquired for each sample. Data analysis is described in the main text. In brief, events were first plotted forward versus side scatter using side scatter on a log scale and a large gate was drawn excluding debris. Events were then plotted for either CD3 or CD11c versus forward scatter area to identify $CD3^+$ T cells and $CD11c^+$ phagocytes. $CD3^+$ and $CD11c^+$ gated cells were then plotted versus the dead cell stain 7-AAD and a live (negatively staining) gate was drawn. Live $CD3^+$ or $CD11c^+$ gated cells were finally plotted either $CD3^+$ (T cells) or $CD11c^+$ (myeloid cells) versus side scatter (SSC log scale). A gate was drawn to identify SSC high cells based on the negative controls.

2.7 Imaging flow cytometry

Imaging flow cytometry analysis was carried out using an ImagesStream^X Mark I platform (Amnis-Merck-Millipore) in standard configuration, equipped with multi-magnification (20X, 40X, 60X), extended depth of field, 405 nm and 488 nm excitation lasers and a 785 nm laser for a scatter signal with standard filter sets. INSPIRE software (Amnis, USA) was used for acquisition and IDEAS software (Amnis, USA) for analysis. Prior to sample acquisition, the machine was calibrated and tested using the standard machine scripts. Cells were filtered through 35 μm nylon cell strainer mesh tubes (BD Biosciences, UK) immediately prior to acquisition and a minimum of 30,000 events per sample were acquired using the 40X objective. The cell classifier was used to set an area upper limit (AUL) of 600 units and an area lower limit (ALL) of 50 units in the brightfield channel to define cellular events, events outside this range were classed as debris and excluded from collection. All channels were collected with the laser power set to 50.0 mW for the 488 nm laser and 3.09 mW for the 785 nm scatter laser. Single stain compensation tubes for each stain used, as well as an unstained tube, were prepared alongside test samples and run for the generation of compensation matrices.

2.7.1 Data analysis guide for measurement of crystalline silica cell association using darkfield bright detail intensity—

A bivariate (dot) plot was first created, using brightfield area versus brightfield aspect ratio to identify single myeloid cell populations and exclude doublets and debris. A single cell gate was then created and a gradient RMS (root mean square) histogram plot of the cells within the single cell gate used to gate on cells in best focus. The gated, single, best-focused cells were then used to create further fluorescence intensity histogram plots of phenotypic markers (*e.g.,* PE-$CD16b^+$ in channel 3 and Alexa-488-$CD14^+$ in channel 2) gating on positive populations as shown in Figure 1. To identify crystalline silica positive cells based on increases in darkfield intensity, the single, focused, fluorescent positive gated cells (*e.g.,* single, focused, PE-$CD16b^+$ gated) were used to create a bivariate plot of the bright detail intensity R3 (BDI R3) in darkfield on the horizontal axis and brightfield on the vertical axis. The negative control (no crystalline silica) sample was used to establish where the natural amount of darkfield signal for the cells resided and the darkfield BDI positive gate was placed *beyond* the natural population cluster for BDI-R3 (see Figure 1B for visual examples). The analysis template was saved so that the same gate (once optimised by the control cells) could be applied to positive samples from

the same donor. This process was repeated for the analysis of every subject to account for subject variations in the cell populations, receptor expression and fluorescence intensities of cells from different donors.

2.7.2 Data analysis guide for measuring crystalline silica internalisation using darkfield images—To identify crystalline silica internalisation as localised increases in darkfield signals, an internalisation mask was created using the erode function in mask manager and eroding the area 4 pixels in from the cell surface staining marker (*e.g.,* for $CD16b^+$ staining neutrophils, erode the channel 2 mask (M02)). With the internalisation mask created, the internalisation feature was then generated using the feature manager, selecting internalisation as the feature, the newly made eroded mask and the darkfield channel (ch 06) for the image channel of interest. Once the internalisation mask and features were created, the single, focused, fluorescent positive gated cell population (*e.g.,* single, focused, PE-$CD16b^+$ gated) was used to create an internalisation histogram, selecting the internalisation feature on the vertical axis, with gates set based on negative controls to establish the baseline darkfield internal signals. This was performed for each different cell type, as darkfield signals vary significantly between cell types depending on their granularity. Examples of internalisation score histograms and the complete gating strategy are shown in Figure 2. The internalisation score combines the strength and localization of a chosen signal, in this case signals in the darkfield channel (ch 6). Therefore, when gated on the entire CD14 or CD16b population of cells (e.g. Figure 2A), the measure includes all darkfield signal negative cells *as well as* membrane-associated darkfield signal positive cells and internalised darkfield positive signal cells within the population. Cells that have a darkfield signal strongly associated with the internal area of the cell *only* appear as having the highest internalisation scores and are classified as having a positive signal through placement of the internalisation high gate (in this analysis the positive gates were set at an internalisation score of just above 3, shown in Figure 2B). For more detail on the successful generation and use of masks in imaging flow cytometry see Dominical *et al.* [29].

2.7.3 Data analysis guide for performing spot counts using darkfield images—To count bright spots appearing within the darkfield images associated with crystalline silica, the existing analysis templates were built on, with the guidance of an analysis wizard, using the existing gated $CD14^+$, $CD16^+$ and DF-BDI high gated populations. The spot count analysis wizard was utilised using the following parameters: The darkfield channel (Ch 06) was used for spot identification; ($CD14^+$ and $CD16b^+$) DF-BDI high gated cells were used as positive truth (i.e. spot positive) populations and a minimum of 100 cells from the $CD14^+$ and $CD16b^+$ populations that were spot *negative* were selected to form the negative truth populations. Using these parameters the spot count wizard identified a spot count peak mask to count bright spots in channel 6 using the following expression: Spot Count_Peak (M06, Channel 6, Bright). Spot to cell background ratios were checked and optimised manually by adjusting the expression in the mask manager and ranged from 13.5 to 15.0 varying by subject. Regions were then set to obtain percentages and images of $CD14^+$ and $CD16b^+$ BDI cells with 0,1,2,3,4 and 5 or more spots identified within the cell.

2.8 Statistics

Groups of data within data sets were initially evaluated for normality using the Shapiro-Wilks test prior to undertaking statistical analysis. Experiments examining crystalline silica cellular association with multiple comparisons were assessed by one way ANOVA and post-hoc analysis using Tukey's Honestly Significant Difference (HSD) method with significance taken as $P < 0.05$. Pearson's product-moment correlation coefficient was applied to evaluate the linear dependence between variables: correlation was considered significant if p values reached 0.01 or less (2-tailed test).

3 Results

3.1 Label-free quantification of crystalline silica association with peripheral blood immune cells using conventional and imaging flow cytometry

Light scattering properties of crystalline silica have previously been used in microscopy and, limitedly, in conventional flow cytometry to identify particle-cell associations, without requiring a particle label or stain [22–25]. Crystalline silica association with immune cells was first assessed using PBMC. Conventional flow cytometry was used to determine whether the crystalline silica particle-induced shifts of SSC light profile were associated with particle dose. PBMC is a mixed population of immune cells, consisting of lymphocytes, monocytes, natural killer cells and dendritic cells derived from peripheral blood. Here, only monocytes/dendritic cells and T lymphocytes, identified by surface expression of CD11c and CD3, respectively, were assessed for silica particle association, as they are the main phagocytic and non-phagocytic immune cell types normally present within these mixed cell populations. PBMC were incubated with increasing concentrations of crystalline silica particles, encompassing the lower end of the concentration ranges used by others [23–25], in TCM for 24 h. The mean SSC intensity of the cells was evaluated using a logarithmic scale, as it better captures large increases in scattering intensities compared to the commonly used SSC linear scale, and a cell death stain (7-AAD) was included in order to exclude signals arising from dead or dying cells (Figure 3A). There was a significant increase in the SSC intensity of the viable monocyte/dendritic cell population, not T lymphocytes, with the concentration of crystalline silica. Concentrations higher than 5 μg/mL crystalline silica resulted in significantly increased SSC profiles of the phagocytic ($CD11c^+$) population but not the lymphocytes (Figure 3B–C). These results show that crystalline silica association with monocytes/dendritic cells can be detected using scattered light signals using conventional flow cytometry, corroborating previous reports [24–25].

We next undertook analyses of crystalline silica challenged PBMC using imaging flow cytometry. The phenotypic staining panel was adjusted so that the monocytes were this time identified by $CD14^+$ expression rather than CD11c. While both markers are used to identify human monocytes [30], the latter is additionally expressed on neutrophils contained within whole blood [31], so the change to CD14 allowed for a panel which could be applied to both PBMC and in whole blood assays. $CD14^+$ monocytes were assessed for silica particle association in response to challenge with increasing doses of crystalline silica particles in TCM for 24 h. After applying a gating strategy similar to that used for conventional flow cytometry, the high-resolution images of each cell acquired by imaging flow cytometry were

carefully analysed. Darkfield image parameters of the single, focused, $CD14^+$ cell population were examined by utilising the bright detail intensity (BDI) feature for the identification and quantitation of bright spots appearing within darkfield images of cells. This feature uses cell masks to compute the intensity of localised bright spots within the area of each cell image. BDI R3 was used in this analysis, which computes the intensity of bright spots that are 3 pixels (roughly 1.5 μm) in radius or less. The BDIs in darkfield (horizontal axis) versus brightfield (vertical axis) of the gated $CD14^+$ cells were plotted to ascertain the number of darkfield BDI high cells in controls and samples exposed to increasing doses of crystalline silica. BDI plots and image examples are shown in Figure 4A. Using this analysis strategy, we found there was a dose-dependent increase in $CD14^+$ gated monocytic cells bearing BDI bright spots in the darkfield channel, where a significant difference from controls was reached at the concentration of 2.5 μg/mL (Figure 4B).

In the previous analyses, only general association, not precise cellular localization, of the crystalline silica particles was assessed. The ability to identify and quantify the localisation (*e.g.,* internalised versus membrane-bound) of crystalline silica is advantageous when investigating the impact of cellular associations, such as inflammation, particle clearance and mechanisms of toxicity. We, therefore, sought to identify particle localization using the images obtained from the imaging flow cytometry analysis. The cross-sectional image of each cell allows the definition of the cell surface membrane, where cell surface markers strongly define the cell perimeter (*e.g.,* the surface-associated receptor staining of CD14, displayed in green, in Figure 4). A custom mask was used to exclude the outer cell membrane providing information on the internal area of the cell. Specifically, the outer edge of the cell image was eroded by 4 pixels, equivalent to 2 μm, to identify crystalline silica (as darkfield signals) in the internal area of the cells. The percentage of $CD14^+$ populations with internalised crystalline silica, identified by increased darkfield BDI measurements, was determined using the internalisation feature (the ratio of intensity inside the cell to the intensity of the entire cell) and each cell was assigned an internalisation score, where higher scores indicate higher internal signal intensities. Histogram plots of internalisation scores for Ch6 (Darkfield/SSC) were used to create internalisation high gates within the gated $CD14^+$ population (visual examples of internalisation histogram plots are shown in Figure 2). These analyses confirmed that crystalline silica internalised by $CD14^+$ monocytes can be identified using this label-free imaging flow cytometry method (Figure 4C). Reassuringly, percentages of $CD14^+$ cells displaying increases in BDI darkfield signals and increases in internalised darkfield signals positively correlated with particle dose, correlation plots are shown in supplementary Figure 2.

3.2 Label-free quantification of crystalline silica association with phagocytes in whole blood by imaging flow cytometry

We next examined cells that had been challenged within fresh whole blood using imaging flow cytometry. Whole blood is a complex biological matrix composed of plasma, red blood cells, white blood cells, and platelets and proteins, any of which might influence cell-particulate interactions. In whole blood, neutrophils are the most abundant immune cell type and have previously been shown to contribute significantly to particle clearance in short term, whole blood cultures [32]. Using recently described approaches [16,32], fresh whole

blood was incubated with crystalline silica in order to test the method using a more realistic and biologically complex matrix. After whole blood was exposed to crystalline silica and incubated for 24 h, red blood cells were lysed, monocyte and neutrophil cells were stained with fluorescent markers and the cell suspensions were analysed by imaging flow cytometry. $CD14^+$ monocytes and $CD16b^+$ neutrophils were assessed for silica particle association as the major phagocytic leucocytes present in circulating blood (and lung tissue after respiratory exposure to crystalline silica) [23,33–34].

Cells were first selected based on area versus aspect ratio of the brightfield cell images, to identify single cells and exclude doublets and debris, followed by a focused gate and a $CD16b^+$ neutrophil or $CD14^+$ monocyte cell marker gate. Darkfield and brightfield imaging parameters of the selected populations were then examined to identify crystalline silica association (gating strategy is shown in Figure 1). The BDI feature was again utilised for the identification and quantitation of bright spots appearing with darkfield images of cells (examples of BDI plots can be found in Figure 1B). The use of imaging flow cytometry allowed for visual comparisons of both the brightfield and corresponding darkfield images. The increased intracellular complexity and granularity of neutrophils appeared evident in the form of increased dark regions (dark spots) in the bright field images (examples are shown in Figure 1B). As would be expected these were increased in areas where a darkfield signal was also present (BDI high gate Figure 1B shown as pink in the BDI plots), but additionally appeared within cells with no associated darkfield signal (shown as blue in the BDI plots), making the brightfield imagery alone less suitable for identifying crystalline silica in the highly granular neutrophil cells.

Dose-dependent increases in $CD14^+$ gated monocytic cells bearing BDI bright spots in the darkfield channel were observed, where a significant difference from controls was reached at the concentration of 25 μg/mL (Figure 5A–B). In the same analysis of $CD16b^+$ gated neutrophils bearing BDI bright spots in the darkfield channel, significance was only reached at the high dose concentration of 250 μg/mL (Figure 5C–D).

The analysis was extended to assess particle localization using the darkfield BDI measurements in both monocytes and neutrophil populations. A custom mask was again generated and used to exclude the outer cell membrane and provide information on the internal area of the cell, examples can be seen on the images shown in Figure 6. Measurement of the percentage of $CD14^+$ and $CD16b^+$ populations with internalised crystalline silica, identified by increased darkfield BDI measurements, were defined using an internalisation feature and assigned an internalisation score. Histogram plots of internalisation scores for Ch6 (Darkfield/SSC) were used to create internalisation high gates within the gated $CD14^+$ and $CD16b^+$ populations (examples of the internalisation score histogram plots are shown in Figure 7). This analysis confirmed the presence of internalised crystalline silica within $CD14^+$ monocytes as anticipated for this highly phagocytic cell type (Figure 6A–B). A significant amount of silica was also found to be internalised by the $CD16b^+$ neutrophil population, but only at the higher concentration tested (Figure 6C–D). Small amounts of crystalline silica were also found associated with the cell membranes of both monocytes and neutrophils.

Since the analysis quantified the amounts of silica particle association simultaneously on both cell types within the mixed leukocyte populations present in whole blood, we were able to examine the phagocytes on a cell by cell basis. Specifically, the whole blood cell composition allowed the comparison of monocytes and neutrophils associating with crystalline silica in terms of real numbers (*i.e.,* as a percentage of the total phagocyte population; monocytes + neutrophils). Figure 8 shows a significantly greater percentage of neutrophil association with crystalline silica when compared to monocytes at the highest concentration. Although monocytes are avid phaocytosers, neutrophils are far more abundant than monocytes in human blood and, as a result, are more likely outcompete monocytes, especially at high silica concentrations. The well-established cytotoxicity of crystalline silica towards monocytes may also contribute to the decreased percentage of monocyte positive cells.

Finally, spot count analyses were performed to examine the individual particle load of both monocyte and neutrophil cells at high and low exposure concentrations. Spot count analyses were performed on the cell populations previously identified as silica particle positive by DF-BDI high signals (Figure 5). An example of gates used to define BDI intensity high in DF are shown in Figure 1B. This further analysis revealed that both monocyte and neutrophil cell types experienced increased cell loading (defined as significantly higher numbers of cells with 5 or more spots) at the higher 250 μg/mL crystalline silica concentration compared to 25 μg/mL ($p = 0.001$ for both $CD14^+$ cells and $CD16b^+$ neutrophils), as might be expected for these professional phagocytic cell types.

4 Discussion and conclusion

Imaging flow cytometry, similar to conventional flow cytometry, is a method by which many cellular parameters can be measured in a robustly quantitative manner. Unlike conventional flow cytometry, imaging flow cytometry also acquires microscopic images of each event (cell) from which more information can be gained. The cell images can be analysed for many different criteria and features which contain both quantitative and positional information relating to the image. Cell masks are used to select specific areas of interest within cells, which can then be used for quantitative and automated analysis of entire or selected (gated) cell populations [29]. When applied to the analysis of native mixed cell populations, realistic insights into particle associations can be measured, assuming that the particle has sufficient properties to allow label-free identification. The method described here, which utilised darkfield reflectance, brightfield, custom cell masks and conventional fluorescent staining, was effective for examining the interactions of single cells with crystalline silica within a complex mixed cell population. We show a method capable of identifying crystalline silica association with phagocytes without the use of labelling while only requiring low sample volumes (e.g. 200 μL of whole blood per sample), making it a promising technique for use analysing *ex vivo* analysis of *in vivo* exposures. However, this method does not distinguish between crystalline silica and other materials with a high capacity to scatter light, such as pigment grade titanium dioxide or crystals of monosodium urate [26,32].

Although reasonably high exposure doses of crystalline silica were used in these experiments, the particles were clearly identifiable, and should also remain identifiable at lower frequencies, although greater numbers of cells would need to be acquired per sample, thus increasing the sample size and running time. Furthermore, a 40X objective was used in these analyses to maximise throughput, greater resolution and sensitivity might be gained from using the 60X objective. Nonetheless, it remains difficult to ascertain exactly how many particles would be encountered by pulmonary cells (either resident or migrating) in a real-life exposure. The UK allows an 8-hour time-weighted averaged workplace exposure limit (WEL) of 0.1 mg/m^3, respirable crystalline silica although a recent report would suggest that these levels are regularly exceeded [35]. From the WEL, daily exposures levels can be calculated using the equations outlined by the Agency for Toxic Substances and Disease Registry (https://www.atsdr.cdc.gov/hac/phamanual/appg.html accessed 2019 Jan 7). For example, an average-sized man (weighing 70 kg) working within this exposure limit for 8 hours could be exposed to as much as 0.35 mg (350 μg) of crystalline silica in a single day (calculations shown in supplementary Figure 3). The extent of particle penetration into the lungs is dependent on particle density, size and airflow, generally with particles $PM^{2.5}$ sized and under capable of reaching the tracheobronchial tract and alveoli whilst particles PM^{10} size and above being too large to reach the lungs [36]. The crystalline quartz material Min-u-sil 5 is mainly a mixture of $PM^{2.5}$ to PM^{10} sized material, with little or no material falling within the ‘nano’ fraction (see supplementary Figure 1). Estimating the likely exposure of phagocyte cells actively mobile within a precise area of the lung is extremely problematic, further complicated by conflicting estimates of the average human lung surface area, the effect of persistent particles accumulating only within specific regions of the lungs, phagocyte migration (into and out of the area and lung) combined with the variables of overall particle persistence and exposure time (days, months, years). Understandably, when it comes to inhaled particulate matter exposure amounts poorly reflect the dose delivered to cells, which varies considerably due to this myriad of factors, with no straightforward accurate way of estimation [37–38]. With this in mind, (and considering levels of persistent particles increasing over the duration of long exposure times in real life exposures), we investigated a range of particle doses using blood as the complex biological matrix and blood-derived phagocytes as target cells. It is likely that particles could be identified within cells obtained from bronchial lavage but this remains to be investigated and should be prioritised in future work. On ice versus 37 °C time course incubations of cells would provide further information relating to membrane bound versus internalisation of the particles and its consequences. Research also suggests that during high-level exposures silica particles travel to multiple sites outside the lung, via the blood and lymphatic systems, which might also serve as possible sample sites [39–40].

It has long been understood that silica dust and particles can act as immunostimulants which cause pulmonary inflammation [23,41–44]. Although the mechanisms beneath these attributes that go beyond the induction of macrophage cell death and innate immune triggering are only beginning to be understood [45–49]. In this current work we found that on a cell-by-cell basis, neutrophils had the greatest association to the silica particles, which would suggest, given their rapid migration to the lung following respirable silica dust exposure, that such associations also occur *in vivo*. Neutrophils and monocytes use Fc

receptors to phagocytose particles and complement-mediated events [50–52]. Phagocytic events can trigger the dynamic secretory and microbicidal activity of neutrophils, specifically the release of microbicidal granules and the release of neutrophil extracellular traps (NETs) [52–53]. Interestingly, several studies have implicated several exogenous particle types, including crystalline silica, in the induction of NET release using freshly isolated neutrophils in short term culture conditions [26,54]. Whilst our current study did not stain for, or examine, NET release by neutrophils, we were able to confirm neutrophil - particle interactions within the whole blood matrix, suggesting that such interactions are likely to occur *in vivo*, either in blood or during periods of neutrophil influx into lung tissue.

We have reported on a fully quantitative imaging flow cytometry assay for the label-free identification and localisation of crystalline silica in association with primary cells, suitable for use *ex vivo* or *in vitro*, including in complex biological matrices. The ability to accurately identify crystalline silica label-free makes it conceivable to apply this technique to the measurement of crystalline silica exposure levels *ex vivo*, or from *in vitro* studies using primary cells in physiologically relevant matrices. Label-free identification avoids changing the attributes of the particles themselves caused by labelling which might otherwise influence cell-particle interactions or outcome. With renewed interest in the role of cell types such as neutrophils contributing to the development of a range of diseases, including multiple auto-immune conditions, the methods reported here might assist future study in this challenging area.

Supplementary Material

Refer to Web version on PubMed Central for supplementary material.

Acknowledgements

This study was funded by UK Medical Research Council, Grant number MR/R005699/1. The authors wish to thank the Volunteer Studies and Clinical Services Team at MRC EWL for recruitment and written consent of volunteers and the volunteers' blood collection.

Abbreviations

PBMC
peripheral blood mononuclear cells

ISX
Imagestream X

DF
darkfield

BF
brightfield

BDI
bright detail intensity

SSC
side scatter

FS
forward scatter

AUL
area upper limit

ALL
area lower limit

gradient RMS
gradient root mean square

WB
whole blood

WEL
workplace exposure limit

NET
neutrophil extracellular trap

7-AAD
7-Aminoactinomycin D

$PM^{0.1}$, $PM^{2.5}$ and PM^{10}
Particulate matter of less than 0.1, 2.5 or 10 μm median aerodynamic diameters

References

1. IARC Working Group on the Evaluation of Carcinogenic Risks to Humans. IARC Monographs on the Evaluation of Carcinogenic Risk of Chemicals to Humans. Vol. 68. Lyon, France: IARCPress; 1997. Silica, Some Silicates, Coal Dust and Para-Armid Fibrils. Available from: https://www.ncbi.nlm.nih.gov/books/NBK410047/
2. Health and Safety Executive Research Report RR878 - Levels of respirable dust and respirable crystalline silica at construction sites. Available from: https://www.hse.gov.uk/research/rrhtm/rr878.htm
3. World Health Organization. Crystalline Silica, Quartz (Concise International Chemical Assessment Document 24). 2000. ISBN-10: 9241530243 Available from: http://www.inchem.org/documents/cicads/cicads/cicad24.htm
4. Pollard KM. Silica, Silicosis, and Autoimmunity. Front Immunol. 2016; 7:97. [PubMed: 27014276]
5. Miller FW, Alfredsson L, Costenbader KH, et al. Epidemiology of environmental exposures and human autoimmune diseases: findings from a National Institute of Environmental Health Sciences Expert Panel Workshop. J Autoimmun. 2012; 39:259–271. [PubMed: 22739348]
6. Bartůňková J, Pelclova D, Fenclová Z, et al. Exposure to silica and risk of ANCA-associated vasculitis. Am J Ind Med. 2006; 49:569–576. [PubMed: 16691610]
7. Pollard KM, Hultman P, Kono DH. Toxicology of autoimmune diseases. Chem Res Toxicol. 2010; 23:455–466. [PubMed: 20078109]

8. Lee S, Matsuzaki H, Kumagai-Takei N, et al. Silica exposure and altered regulation of autoimmunity. Environ Health Prev Med. 2014; 19:322–329. [PubMed: 25135741]
9. Van der Woude FJ, Lobatto S, Permin H, et al. Autoantibodies against neutrophils and monocytes. Tool for diagnosis and marker of disease activity in Wegener's granulomatosis. Lancet. 1985; 325:425–429.
10. Germolec D, Kono DH, Pfau JC, et al. Animal models used to examine the role of the environment in the development of autoimmune disease: findings from an NIEHS Expert Panel Workshop. J Autoimmun. 2012; 39:285–293. [PubMed: 22748431]
11. Riediker M, Zink D, Kreyling W, et al. Particle toxicology and health-where are we? Part Fibre Toxicol. 2019; 16:19. [PubMed: 31014371]
12. Murphy CJ, Vartanian AM, Geiger FM, et al. Biological responses to engineered nanomaterials: Needs for the next decade. ACS Central Sci. 2015; 1:117–123.
13. Fröhlich E. Value of phagocyte function screening for immunotoxicity of nanoparticles in vivo. Int J Nanomed. 2015; 10:3761–3778.
14. Jochums A, Friehs E, Sambale F, et al. Revelation of Different Nanoparticle-Uptake Behavior in Two Standard Cell Lines NIH/3T3 and A549 by Flow Cytometry and Time-Lapse Imaging. Toxics. 2017; 5:15.
15. Parks CG, Miller FW, Pollard KM, et al. Expert panel workshop consensus statement on the role of the environment in the development of autoimmune disease. Int J Mol Sci. 2014; 15:14269–14297. [PubMed: 25196523]
16. Baumann D, Hofmann D, Nullmeier S, et al. Complex encounters: nanoparticles in whole blood and their uptake into different types of white blood cells. Nanomedicine. 2013; 8:699–713. [PubMed: 22934978]
17. Vranic S, Boggetto N, Contremoulins V, et al. Deciphering the mechanisms of cellular uptake of engineered nanoparticles by accurate evaluation of internalization using imaging flow cytometry. Part Fibre Toxicol. 2013; 10:2. [PubMed: 23388071]
18. Phanse Y, Ramer-Tait AE, Friend SL, et al. Analyzing cellular internalization of nanoparticles and bacteria by multi-spectral imaging flow cytometry. J Vis Exp. 2012; 64:e3884.
19. Rieger AM, Hall BE, Barreda DR. Macrophage activation differentially modulates particle binding, phagocytosis and downstream antimicrobial mechanisms. Dev Comp Immunol. 2010; 34:1144–1159. [PubMed: 20600280]
20. Marangon I, Boggetto N, Ménard-Moyon C, et al. Localization and relative quantification of carbon nanotubes in cells with multispectral imaging flow cytometry. J Vis Exp. 2013; 82:e50566.
21. Smirnov A, Solga MD, Lannigan J, et al. An improved method for differentiating cell-bound from internalized particles by imaging flow cytometry. J Immunol Methods. 2015; 423:60–69. [PubMed: 25967947]
22. Tian L, Dai S, Wang J, et al. Nanoquartz in Late Permian C1 coal and the high incidence of female lung cancer in the Pearl River Origin area: a retrospective cohort study. BMC Public Health. 2008; 8:398. [PubMed: 19055719]
23. Hornung V, Bauernfeind F, Halle A, et al. Silica crystals and aluminum salts activate the NALP3 inflammasome through phagosomal destabilization. Nat Immunol. 2008; 9:847–856. [PubMed: 18604214]
24. Beamer CA, Holian A. Scavenger receptor class A type I/II (CD204) null mice fail to develop fibrosis following silica exposure. Am J Physiol Lung Cell Mol Physiol. 2005; 289:L186–L195. [PubMed: 15849212]
25. Beamer GL, Seaver BP, Jessop F, et al. Acute exposure to crystalline silica reduces macrophage activation in response to bacterial lipoproteins. Front Immunol. 2016; 7:49. [PubMed: 26913035]
26. Schorn C, Janko C, Latzko M, et al. Monosodium urate crystals induce extracellular DNA traps in neutrophils, eosinophils, and basophils but not in mononuclear cells. Front Immunol. 2012; 3:277. [PubMed: 22969769]
27. Satpathy SR, Jala VR, Bodduluri SR, et al. Crystalline silica-induced leukotriene B4-dependent inflammation promotes lung tumour growth. Nat Commun. 2015; 6
28. Chubb LG, Cauda EG. Characterizing particle size distributions of crystalline silica in gold mine dust. Aerosol Air Qual Res. 2017; 17:24–33. [PubMed: 28217139]

29. Dominical V, Samsel L, McCoy JP Jr. Masks in imaging flow cytometry. Methods. 2017; 112:9–17. [PubMed: 27461256]
30. Boyette LB, Macedo C, Hadi K, et al. Phenotype, function, and differentiation potential of human monocyte subsets. PLoS One. 2017; 12:e0176460. [PubMed: 28445506]
31. Rosales C. Neutrophil: A cell with many roles in inflammation or several cell types? Front Physiol. 2018; 9:113. [PubMed: 29515456]
32. Hewitt RE, Vis B, Pele LC, et al. Imaging flow cytometry assays for quantifying pigment grade titanium dioxide particle internalization and interactions with immune cells in whole blood. Cytom Part A. 2017; 91:1009–1020.
33. Sellamuthu R, Umbright C, Roberts JR, et al. Blood gene expression profiling detects silica exposure and toxicity. Toxicol Sci. 2011; 122:253–264. [PubMed: 21602193]
34. Ishihara Y, Yasuhara T, Ishiyama S, et al. The role of leukocytes during acute phase inflammation in crystalline silica-induced lung injury. Exp Lung Res. 2001; 27:589–603. [PubMed: 11597119]
35. Baldwin PEJ, Yates T, Beattie H, et al. Exposure to Respirable Crystalline Silica in the GB Brick Manufacturing and Stone Working Industries. Ann Work Expos Health. 2019; 63:184–196.
36. Künzli N, Perez L, Rapp R. Air quality and health. Lausanne: European Respiratory Society. World Health Organ. 2010; 89
37. Schmid O, Cassee FR. On the pivotal role of dose for particle toxicology and risk assessment: exposure is a poor surrogate for delivered dose. Part Fibre Toxicol. 2017; 14:52. [PubMed: 29216928]
38. Fröhlich E, Mercuri A, Wu S, et al. Measurements of deposition, lung surface area and lung fluid for simulation of inhaled compounds. Front Pharmacol. 2016; 7:181. [PubMed: 27445817]
39. Friedetzky A, Garn H, Kirchner A, et al. Histopathological changes in enlarged thoracic lymph nodes during the development of silicosis in rats. Immunobiology. 1998; 199:119–132. [PubMed: 9717672]
40. Xu M, Qing M, Peng D. Silicon dioxide particles deposited in vessels and cartilage of the femoral head. Yonsei Med J. 2014; 55:1447–1449. [PubMed: 25048510]
41. Slavin RE, Swedo JL, Brandes D, et al. Extrapulmonary silicosis: a clinical, morphologic, and ultrastructural study. Hum Pathol. 1985; 16:393–412. [PubMed: 3980008]
42. Chu Z, Huang Y, Li L, et al. Physiological pathway of human cell damage induced by genotoxic crystalline silica nanoparticles. Biomaterials. 2012; 33:7540–7546. [PubMed: 22795858]
43. Ueki A, Yamaguchi M, Ueki H, et al. Polyclonal human T-cell activation by silicate in vitro. Immunology. 1994; 82:332. [PubMed: 7927506]
44. Wu P, Hyodoh F, Hatayama T, et al. Induction of CD69 antigen expression in peripheral blood mononuclear cells on exposure to silica, but not by asbestos/chrysotile-A. Immunol Lett. 2005; 98:145–152. [PubMed: 15790520]
45. Braakhuis HM, Park MVDZ, Gosens I, et al. Physicochemical characteristics of nanomaterials that affect pulmonary inflammation. Part Fibre Toxicol. 2014; 11:18. [PubMed: 24725891]
46. Vis B, Hewitt RE, Faria N, et al. Non-functionalized ultrasmall silica nanoparticles directly and size-selectively activate T cells. ACS Nano. 2018; 12:10843–10854. [PubMed: 30346692]
47. Vis B, Hewitt RE, Monie TP, et al. Ultrasmall silica nanoparticles directly ligate the T cell receptor complex. P Natl Acad Sci. 2020; 117:285–291.
48. Eleftheriadis T, Pissas G, Zarogiannis S, et al. Crystalline silica activates the T-cell and the B-cell antigen receptor complexes and induces T-cell and B-cell proliferation. Autoimmunity. 2019; 52:136–143. [PubMed: 31119949]
49. Hewitt RE, Chappell HF, Powell JJ. Small and dangerous? Potential toxicity mechanisms of common exposure particles and nanoparticles. Curr Opin Toxicol. 2020; 19:93–98. [PubMed: 32566804]
50. Gilberti RM, Joshi GN, Knecht DA. The phagocytosis of crystalline silica particles by macrophages. Am J Resp Cell Mol Biol. 2008; 39:619–627.
51. Pacheco P, White D, Sulchek T. Effects of microparticle size and Fc density on macrophage phagocytosis. PLoS One. 2013; 8:e60989. [PubMed: 23630577]

52. Dale DC, Boxer L, Liles WC. The phagocytes: neutrophils and monocytes. Blood, J Am Soc Hematol. 2008; 112:935–945.

53. Brinkmann V, Zychlinsky A. Neutrophil extracellular traps: is immunity the second function of chromatin? J Cell Biol. 2012; 198:773–783. [PubMed: 22945932]

54. Desai J, Foresto-Neto O, Honarpisheh M, et al. Particles of different sizes and shapes induce neutrophil necroptosis followed by the release of neutrophil extracellular trap-like chromatin. Sci Rep. 2017; 7

Europe PMC Funders Author Manuscripts

Europe PMC Funders Author Manuscripts

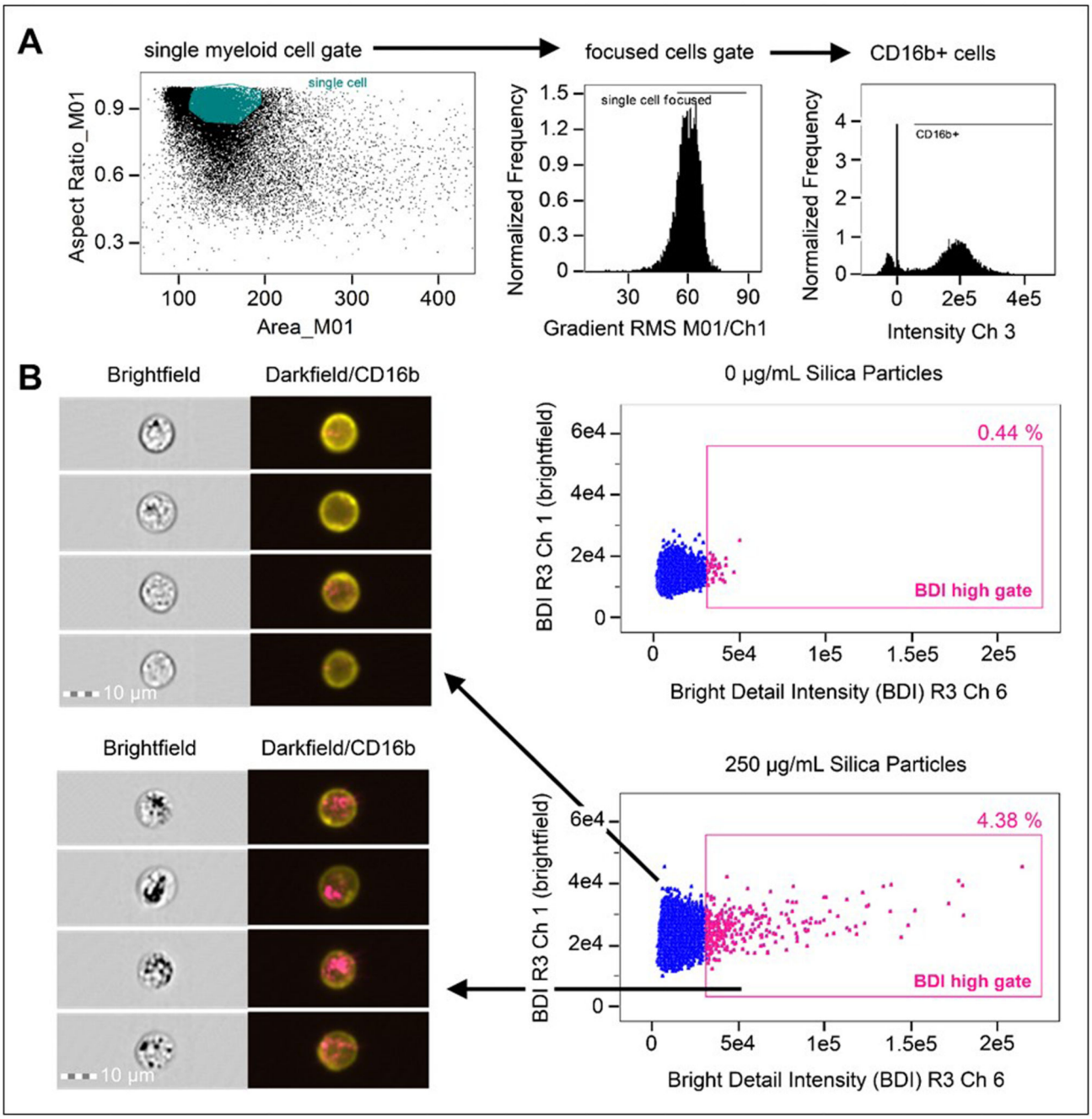

Figure 1. Analysis strategy for the identification of crystalline silica association with phagocytes in whole blood using brightfield and darkfield parameters A.

Area (size of the masked cells in μm^2) versus aspect ratio (of the minor axis divided by the major axis) of the brightfield cell images were used to draw an initial dot plot to identify cells of interest and exclude doublets and debris. From the single cell (phagocyte) gate, cells in best focus were gated (using gradient RMS), followed by gating $CD16b^+$ positive cells based on their fluorescence intensity (histograms for $CD16b^+$ in Ch 3). B. Single, focused, gated $CD16b^+$ cells were then plotted as bivariate plots using bright detail intensity (BDI) measurements for brightfield (vertical axis) and darkfield (horizontal axis). A region

selecting cells displaying increases in darkfield (Ch 6) BDI was then drawn based on the 0 ug/mL particle control. Representative brightfield and merged darkfield (pink)/ $CD16b^{+}$ fluorescence (yellow) image examples of the cells residing within gates (pink dots) and outside BDI high gates (blue dots) are shown.

Europe PMC Funders Author Manuscripts

Europe PMC Funders Author Manuscripts

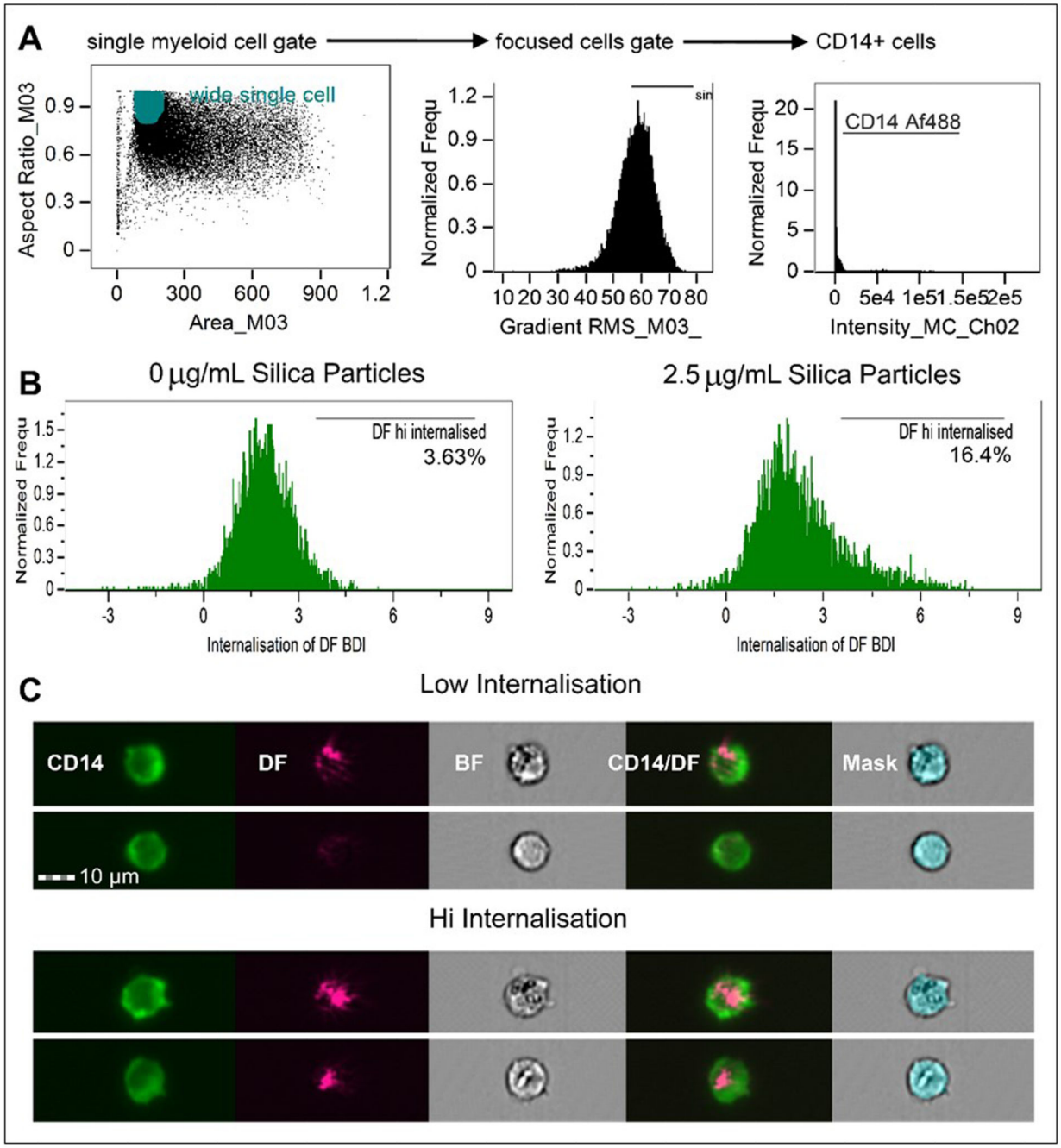

Figure 2. Analysis strategy and histogram plots of internalisation scores for Ch6 (Darkfield/SSC) and internalisation hi gates of gated CD14$^+$ populations within PBMC.

A. Area (size of the masked cells in µm^2) versus aspect ratio (of the minor axis divided by the major axis) of the brightfield cell images were used to draw an initial dot plot to identify cells of interest and exclude doublets and debris. From the single cell (phagocyte) gate, cells in best focus were gated (using gradient RMS), followed by gating on CD14$^+$ positives using fluorescence intensity in Ch02. Examples are shown from the analysis of 1 subject. B. Using the single, focused, CD14$^+$ gates, the IDEAS internalisation feature was utilised to create internalisation score histograms for the single, focused CD14$^+$ gated cells. Internalisation hi

gates were then drawn to establish the number of cells displaying highly internalised darkfield intensity signals. C. Representative example images of cells scoring as having high and low internalisation of particle.

Europe PMC Funders Author Manuscripts

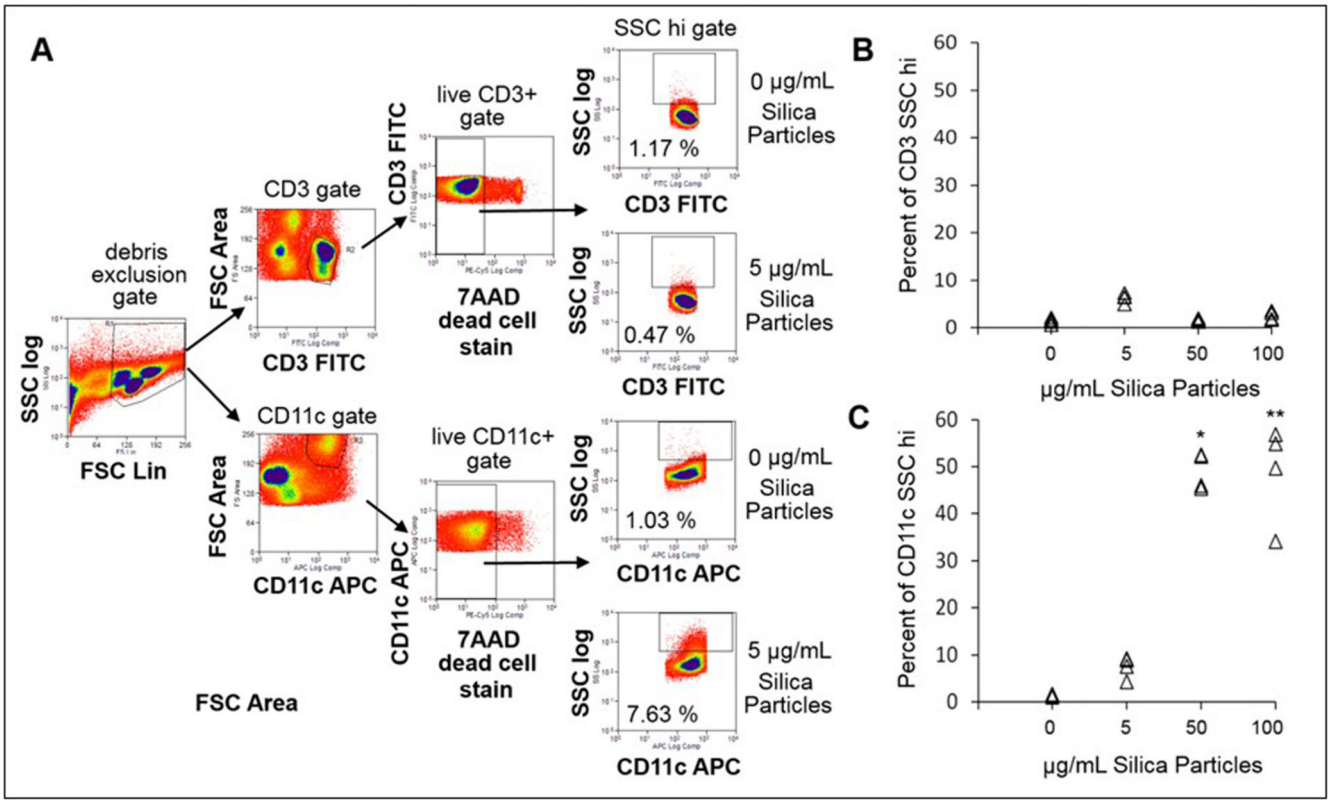

Figure 3. Identification of crystalline silica particle association with cells in PBMC by conventional flow cytometry.

A. Flow cytometry gating strategy. Cells were plotted forward scatter (FSC) versus SSC (log scale), a large gate was drawn excluding debris, followed by plots for either CD3 or CD11c versus FSC area to identify $CD3^+$ T cell and $CD11c^+$ phagocytes. $CD3^+$ and $CD11c^+$ gated cells were then plotted versus the dead cell stain 7-AAD and a live (negatively staining) gate drawn. Live $CD3^+$ or $CD11c^+$ gated cells were finally plotted $CD3^+$ or $CD11c^+$ versus SSC (log scale). A gate was drawn to identify SSC high cells based on the negative controls (0 µg/mL). B. Percentage of $CD3^+$ lymphocytes cells and C. $CD11c^+$ phagocytes gated as SSC intensity high with increasing dose of crystalline silica in PBMC of n = 4 individual subjects. A significant difference from the control was assessed using Tukey's honest significance test for multiple comparisons following a one way ANOVA. * p = 0.001 and ** p = 0.001.

Europe PMC Funders Author Manuscripts

Europe PMC Funders Author Manuscripts

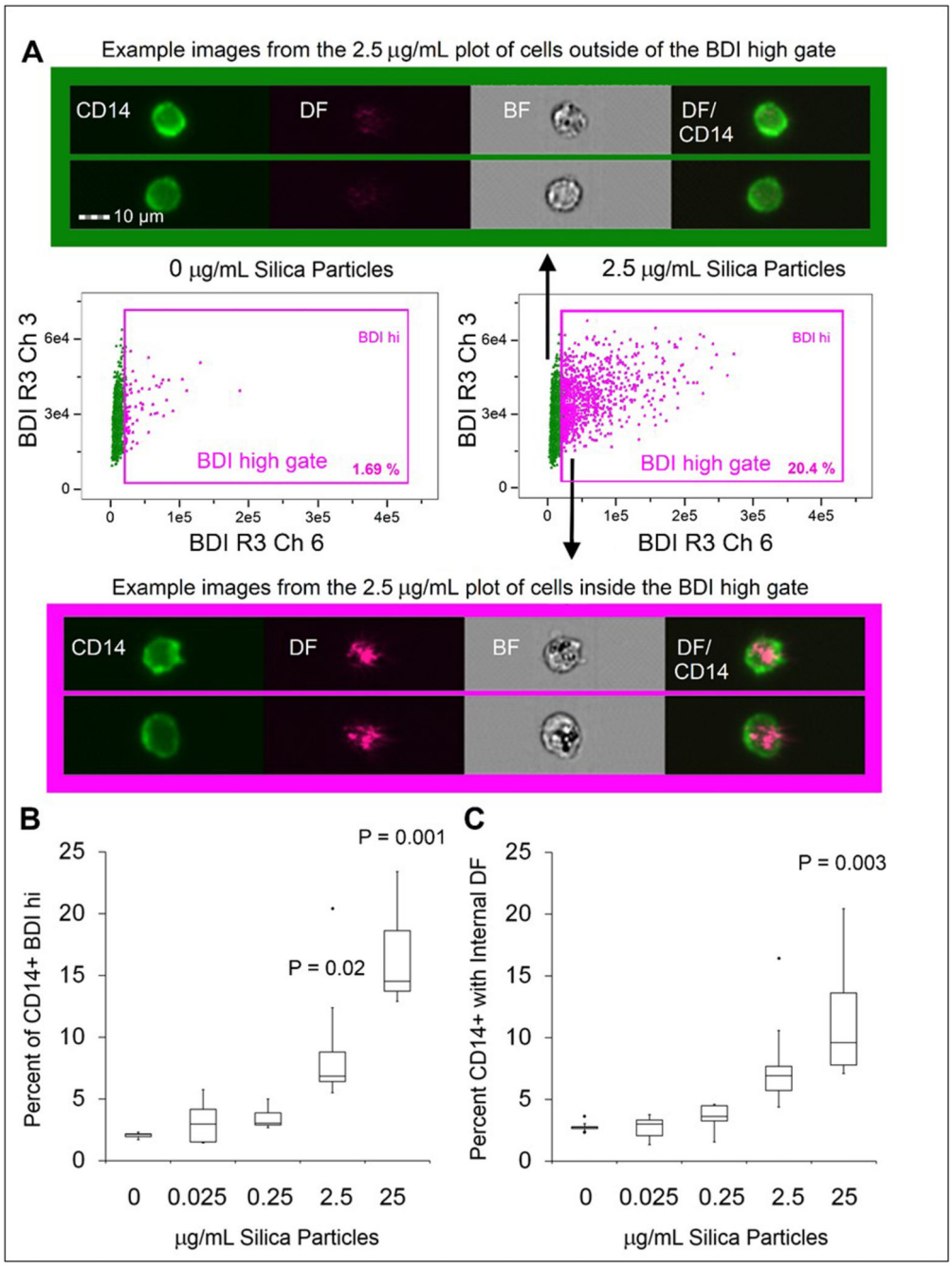

Figure 4. Imaging flow cytometry label-free measurement of crystalline silica particle association with cells in PBMC.

A. Example bivariate plot and representative image examples of focused, single, $CD14^+$ gated cells BDI measurements for brightfield (Ch 03, vertical axis) and darkfield (Ch06, horizontal axis), data from 1 concentration with the control cells from 1 donor are shown. The full gating strategy can be found in Figure 2A. B. Percentage of $CD14^+$ monocytes within PBMC displaying a high DF-BDI signal after incubation with increasing concentrations of crystalline silica (n = 5 subjects). C. Percentage of $CD14^+$ monocytes within PBMC displaying an internalised DF-BDI signal after incubation with increasing

concentrations of crystalline silica (n = 5 subjects). A significant difference from the control was assessed using Tukey's honest significance test for multiple comparisons following a one way ANOVA, p values are shown on the graph were significant. Boxplots display Q1-Q3 with whiskers set at 1.5 x IQR (interquartile range) above the third quartile and 1.5 x IQR below the first quartile, minimum or maximum values that have fallen outside this range are shown as outliers (small black dots).

Europe PMC Funders Author Manuscripts

Europe PMC Funders Author Manuscripts

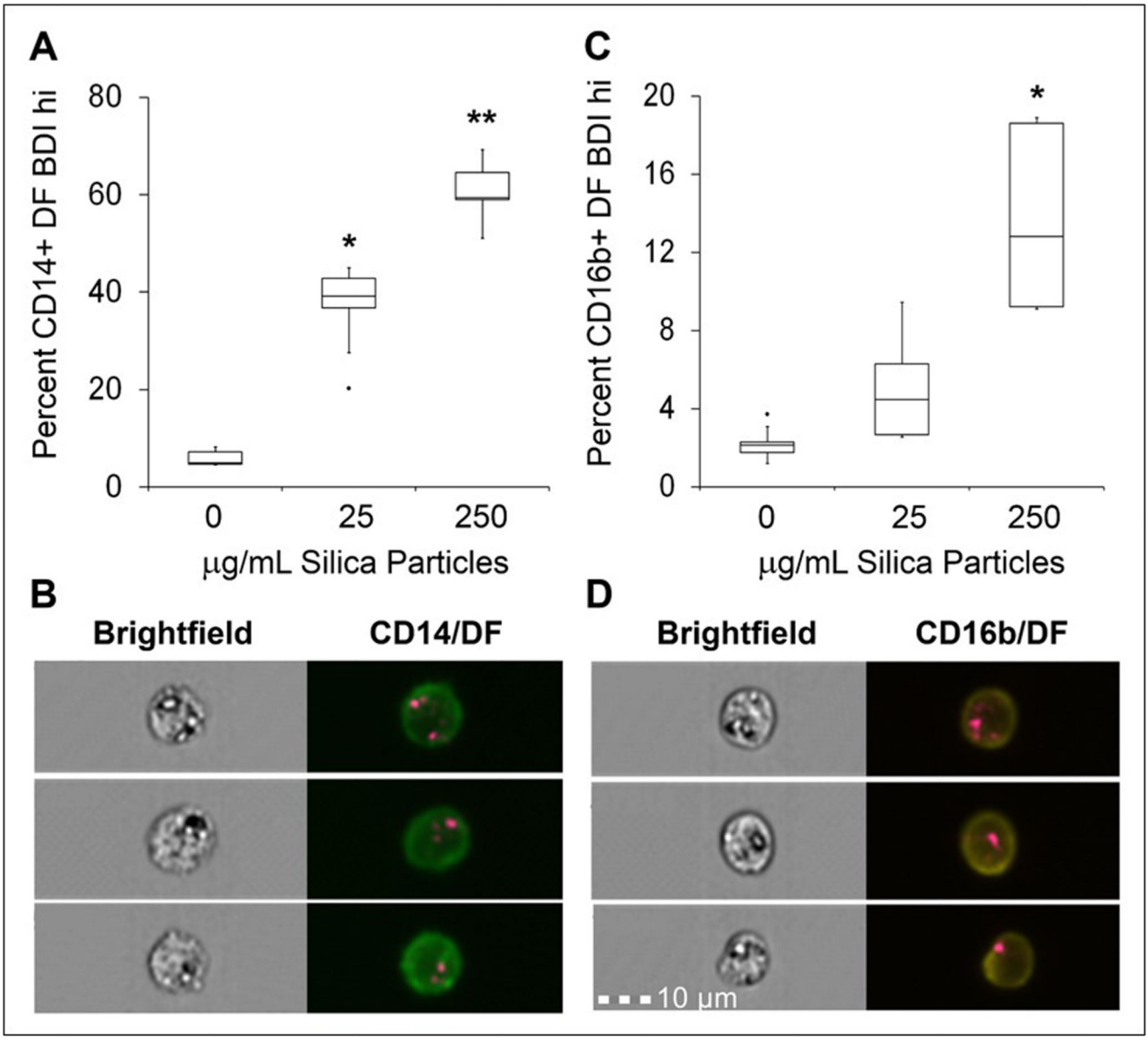

Figure 5. Imaging flow cytometry label-free measurement of crystalline silica particle association with phagocytes in whole blood.

A. Percentage of $CD14^+$ monocytes displaying a high DF-BDI signal after incubation with crystalline silica in whole blood (n = 5 subjects), * p = 0.001 and ** p = 0.001, representative image examples of $CD14^+$ DF-BDI cells from one donor are shown in B. C. Percentage of $CD16^+$ neutrophils displaying a high DF-BDI signal after incubation with crystalline silica in whole blood (n = 5 subjects), * p = 0.001, representative image examples of $CD16b^+$ DF-BDI cells from one donor are shown in D. Significant difference from the control was assessed using Tukey's honest significance test for multiple comparisons following a one way ANOVA. Boxplots display Q1-Q3 with whiskers set at 1.5 x IQR (interquartile range) above the third quartile and 1.5 x IQR below the first quartile, minimum

or maximum values that have fallen outside this range are shown as outliers (small black dots).

Europe PMC Funders Author Manuscripts

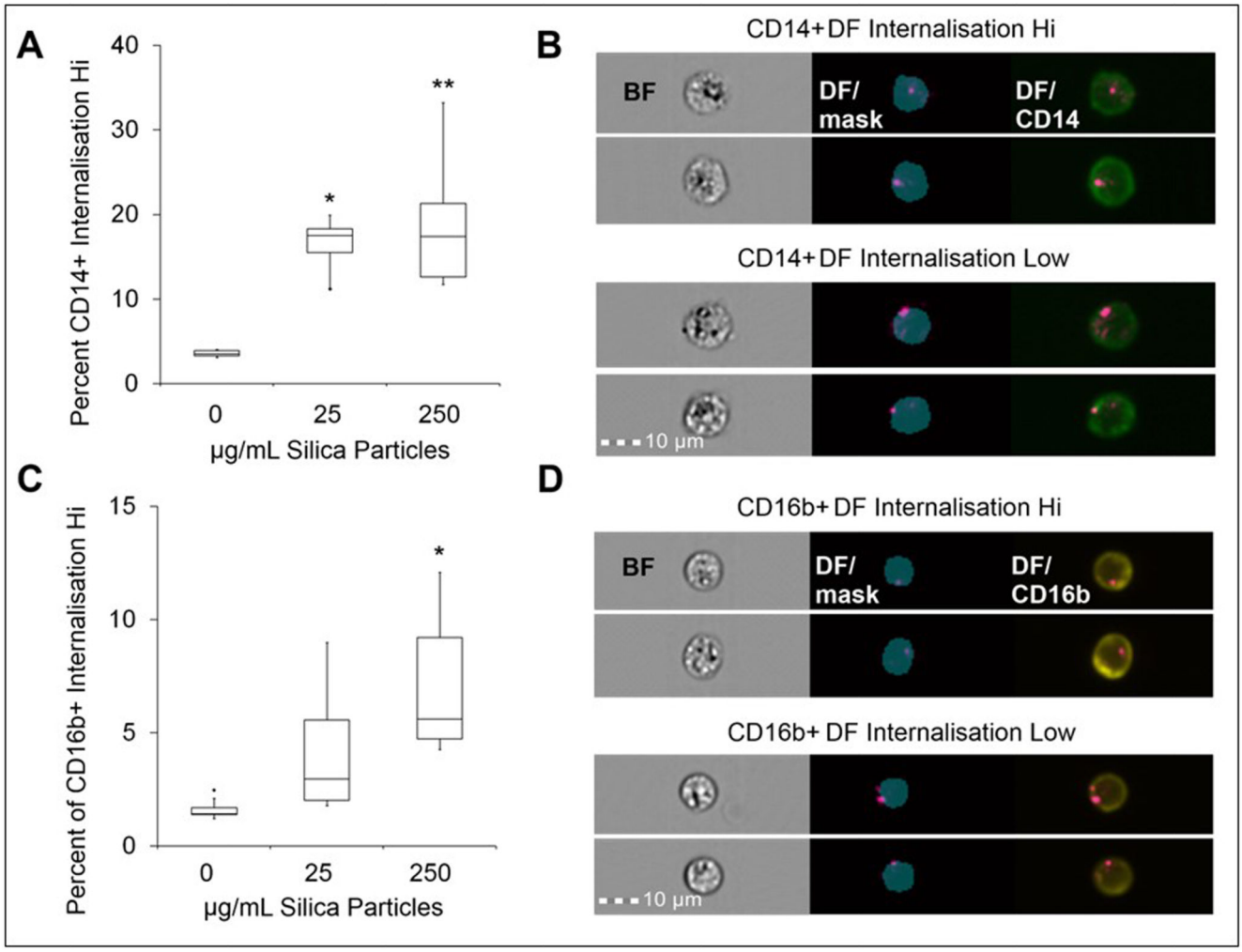

Figure 6. Neutrophil and monocyte internalisation of crystalline silica in whole blood by imaging flow cytometry.

A. Percentage of $CD14^+$ monocytes displaying a high DF-BDI signal gated as internalisation high by imaging flow analysis after incubation with crystalline silica in whole blood (n = 5 subjects), * p = 0.006 and ** p = 0.001. B. Example analysis images of $CD14^+$ (green) cells; brightfield (BF), merged DF and internalisation mask (blue) and merged DF/CD14 cell images are shown (from left to right) for examples of internalisation high and low $CD14^+$ cells. C. Percentage of $CD16b^+$ neutrophils displaying a high DF-BDI signal gated as internalisation high by imaging flow analysis after incubation with crystalline silica in whole blood (n = 5 subjects), * p = 0.01. D. Example analysis images of $CD16b^+$ (yellow) cells; BF, merged DF and internalisation mask (blue) and merged DF/CD16 cell example images of internalisation high and low $CD16b^+$ cells are shown. Boxplots display Q1-Q3 with whiskers set at 1.5 x IQR (interquartile range) above the third quartile and 1.5 x IQR below the first quartile, minimum or maximum values that have fallen outside this range are shown as outliers (small black dots). A significant difference from the control was assessed using Tukey's honest significance test for multiple comparisons following a one way ANOVA.

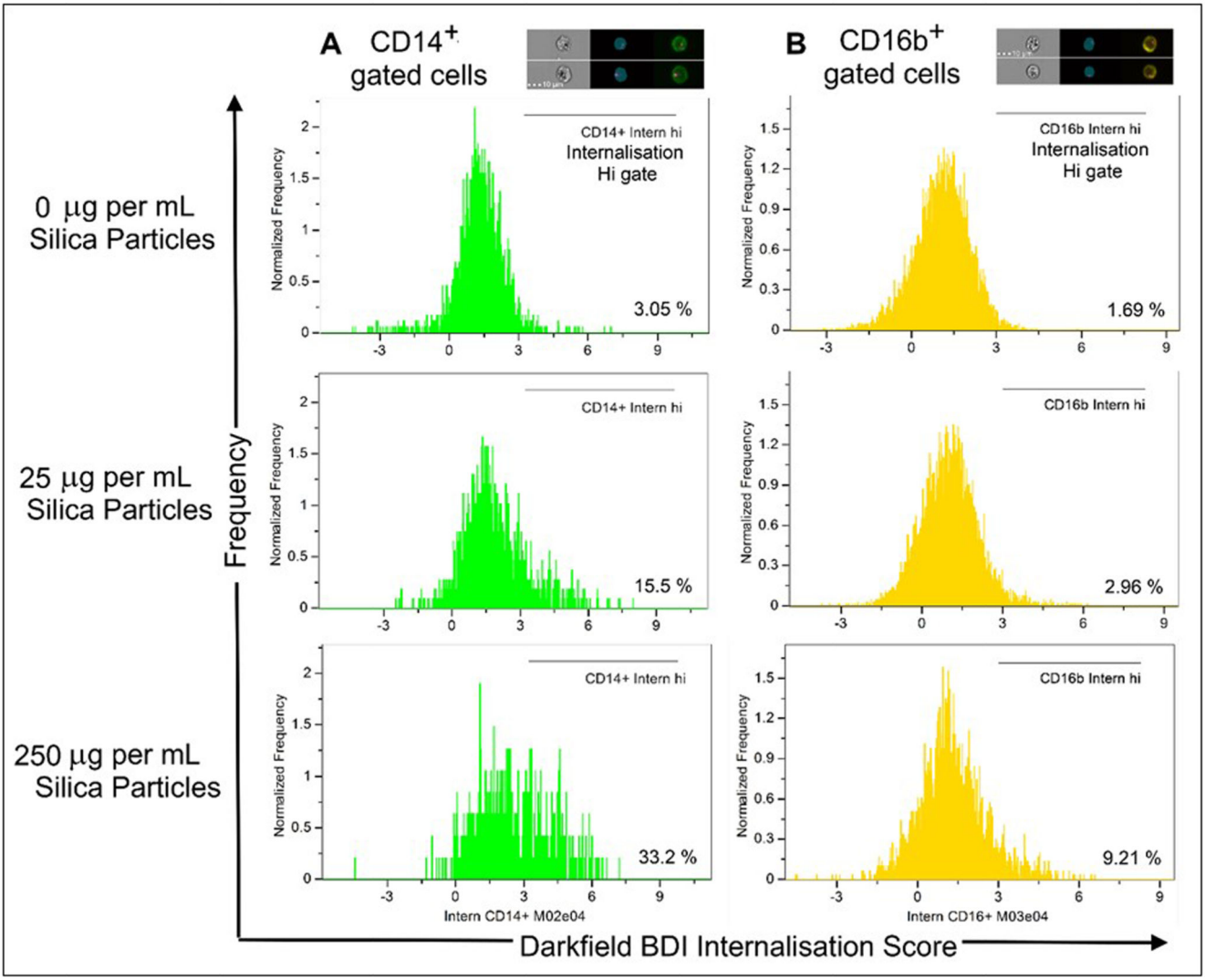

Figure 7. Histogram plots of internalisation scores for Ch6 (Darkfield/SSC) and internalisation high gates of gated CD14$^+$ and CD16b$^+$ populations present in whole blood.

A. Examples are shown from the analysis of 1 subject. Using the single, focused, CD16b$^+$ or CD14$^+$ gates (shown in Figure 1), the IDEAS internalisation feature was utilised to create internalisation score histograms for the single, focused CD14$^+$ gated cells and B. single, focused, CD16b$^+$ cells. Internalisation hi gates were then drawn to establish the number of cells displaying highly internalised darkfield intensity signals. Experimental set up and acquisition was carried out as described within the main text.

Europe PMC Funders Author Manuscripts

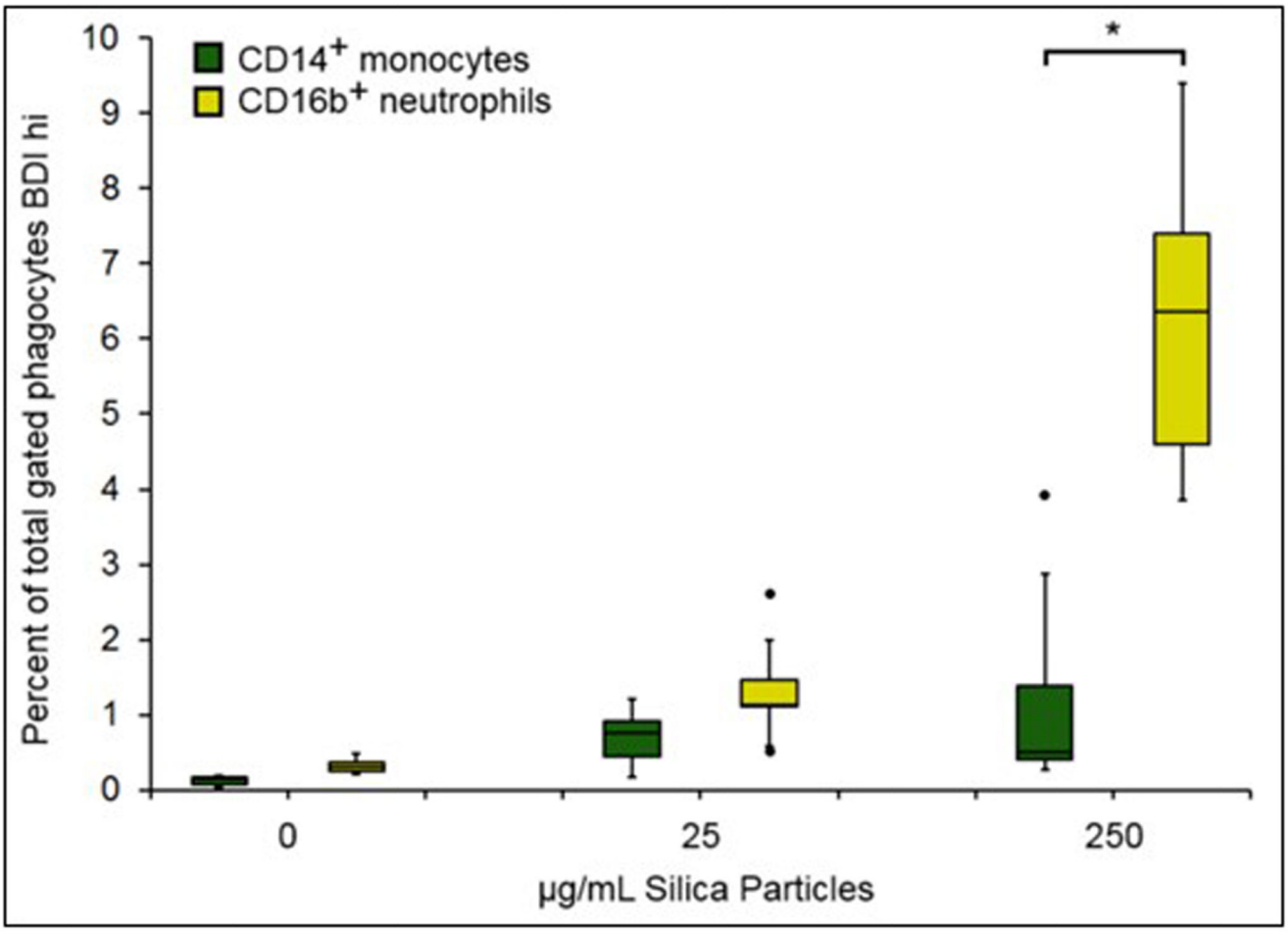

Figure 8. Crystalline silica association with monocytes and neutrophils on a cell by cell basis.

Association crystalline silica with monocytes and neutrophils expressed as the percentage of total gated phagocytic cells by ISX analysis. Percentage of $CD14^+$ monocytes (green) and $CD16b^+$ neutrophils (yellow) gated as darkfield bright detail intensity high (BDI high) expressed as a percentage of the total gated cells (single phagocyte/focused cell gate) in whole blood incubations with crystalline silica (n = 5 individual subjects). Boxplots display Q1-Q3 with whiskers set at 1.5 x IQR (interquartile range) above the third quartile and 1.5 x IQR below the first quartile, minimum or maximum values that have fallen outside this range are shown as outliers (small black dots). A significant difference between monocytes and neutrophils at each concentration was assessed using Tukey's honest significance test for multiple comparisons following a one way ANOVA. * p = 0.001.

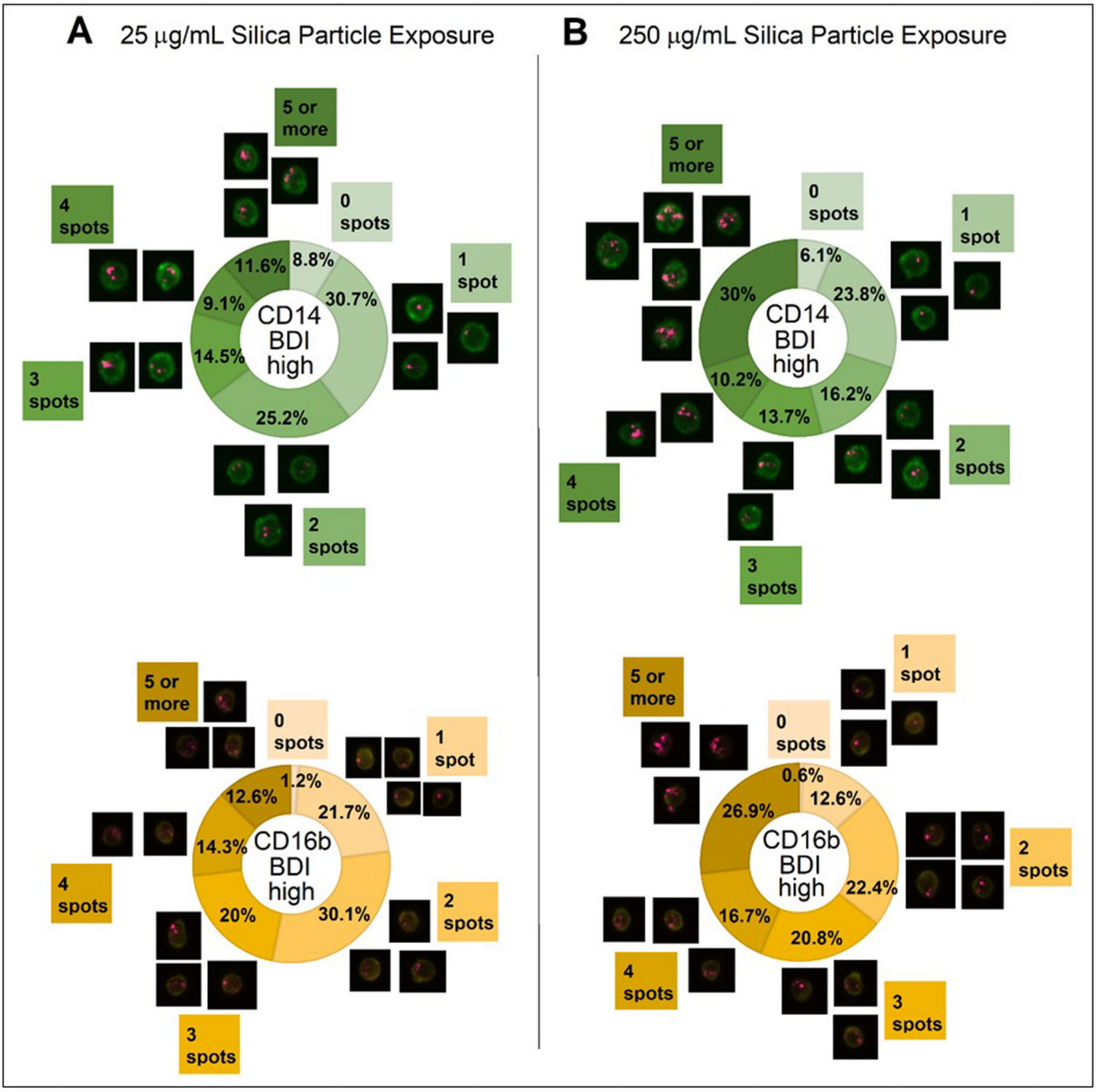

Figure 9. Crystalline silica particle loading of monocytes and neutrophils on a cell by cell basis.

Measurement of the number of individual bright spots in darkfield BDI appearing in cells after exposure to 25 and 250 µg/mL crystalline silica particles carried out using spot count analyses of the darkfield BDI high gated cells. Percentages of cells bearing 0, 1, 2, 3, 4 and 5 (or more) spots are displayed as doughnut charts with adjacent image examples for each segment for $CD14^+$ monocytes (green) and $CD16b^+$ neutrophils (yellow) exposed for 24 h to A. 25 µg/mL and B. 250 µg/mL crystalline silica particles in whole blood incubations (averaged data of n = 5 individual subjects). A significant difference in the number of spots

between concentrations was assessed using Tukey's honest significance test for multiple comparisons following a one way ANOVA.

Europe PMC Funders Author Manuscripts